

S. Slouma^{1,3,*}
S. Skander
Mustapha^{1,2},
I. Slama
Belkhodja¹,
M.Orabi⁴

J. Electrical Systems 11-2 (2015): 145-159

Regular paper

An improved simple Fuel Cell model for Energy Management in residential buildings



This paper deals with a fuel cell (FC) model to be integrated into the energy management algorithm for a stand-alone residential photovoltaic (PV) power system. The FC system is added to guarantee continuous power supply taking account of the photovoltaic intermittent nature. FC models are generally relatively complex especially when they should be introduced in a complete hybrid system model. This paper investigates a simple FC model derived from the FC electrical circuit model. Analytic expression of each element of this simple circuit is established. Experimental tests are conducted to identify the model parameters. FC model is simulated using PSIM software and validated with corresponding experimental polarization curves. To verify FC model effectiveness for energy management algorithm, simulations are carried out with specific load shape and a hybrid system (FC and PV systems with storage batteries). Several scenarios are performed under various meteorological conditions and in case of non-availability generation.

Keywords: Fuel Cell model; Hybrid system; Photovoltaic; Energy management; control.

Article history: Received 10 October 2014, Received in revised form 11 January 2015, Accepted 24 April 2015

1. Introduction

Over the past years, there has been a real increase in the use of DC supply specially, for residential applications. This is due to the increased energy saving and the improved reliability[1], and the significant portion of the used residential load operating with DC current, such as lighting applications, multimedia, computers and all devices operating internally on DC.

Hence, DC power sources as photovoltaic system (PVS) directly coupled to DC loads seem to be a reasonable solution for residential buildings. However, several factors should be considered: First, PVS are highly depending on daily and seasonally climatic conditions variations. In addition, a large part of domestic loads has minor coincidence with PVS output. Furthermore, the load shape is less foreseeable due to residential appliances and users behaviours.

In order to overcome these problems and to improve hybrid system reliability, PVS can be associated with other alternate power sources, like fuel cell system (FCS) as described in [1]- [4]. When there is a deficit in PV power generation, the FCS will intervene to produce energy. In fact, associating PVS with fuel cells for residential applications leads to a non-polluting and reliable energy source. In addition, FC systems are in their advanced developmental stage, they present a promising electrical power source for applications such as electric vehicles, emergency power systems and domestic devices [5]-[7]. Amongst the various available fuel cells, Proton Exchange Membrane Fuel Cells (PEMFC) are regarded

* Corresponding author: S. Slouma, Université de Tunis El Manar, Ecole Nationale d'Ingénieurs de Tunis, LR11ES15 Laboratoire de Systèmes Electriques, 1002, Tunis, Tunisie, E-mail: safa.slouma@crten.rnrt.tn

¹ Université de Tunis El Manar, Ecole Nationale d'Ingénieurs de Tunis, LR11ES15 Laboratoire de Systèmes Electriques, 1002, Tunis, Tunisia

² Université de Carthage, Ecole Nationale d'Architecture et d'Urbanisme, 2026, Sidi Bou Said, Tunisia

³ Technopôle Borj Cédria, Centre de Recherche et de Technologie de l'Energie, LR10CRTE01 Laboratoire Photovoltaïque, 2050, Tunisia

⁴ APEARC, Dept. of Electrical Engineering, Faculty of Engineering in Aswan, South-Valley University, Egypt

as one of the most suitable for residential applications due to their low operating temperature, high efficiency, quick response, and zero emission of gases [5]-[7].

Different FCS models are reported in literature [8]-[12]. These models are relatively complex due to the FC non-linear electrochemical and mechanical characteristics [8]-[10]. These complexities are especially due to the analytic equations related to each of membrane resistance equation and activation voltage drop. For example, in [1],[10], the membrane resistance equation contains a relatively complicated resistivity numeric expression. In the same way in [9],[10], [11],[13], the activation voltage drop is calculated by a relatively complex expression using parametric coefficients. Those coefficients are also themselves based on theoretical equations, including a complex term of oxygen concentration.

In this paper, authors focus on the design of a simple FC model, to be used for the stand-alone residential energy management system. The overall power management strategy is designed to ensure continuous supply whatever specific residential load shape and meteorological conditions fluctuations. The developed FC model is integrated in a whole hybrid system and validated experimentally.

This paper is organized as follows: firstly a description of the overall system is completed; then, model and detailed control process of each component are performed. Simulations are carried out to verify the effectiveness of the proposed system. Next, experimental validation of FC model is presented. Finally a power management algorithm for the residential application and a hybrid system (FC and PV systems with storage batteries) is achieved using the developed FC model. Several scenarios are performed under various meteorological conditions and in case of non-availability generation.

2. System description and modelling

The proposed hybrid system (Fig. 1) is composed of PVS associated to a FCS supplied by a hydrogen storage tanks. A supplementary battery storage system is introduced.

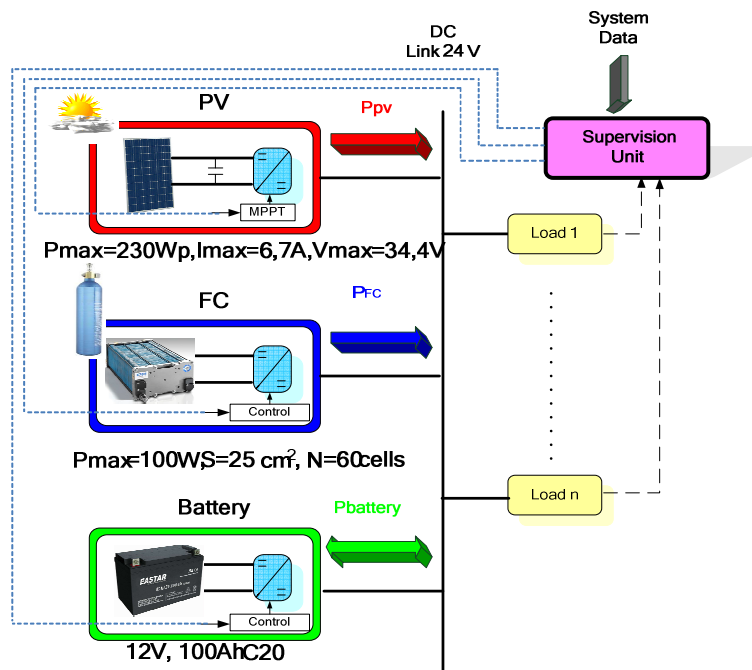


Fig. 1. Overall hybrid system.

A supervision unit including the energy management algorithm is performed to achieve continuous supply of load demand. Each component is detailed as follows:

2.1. Photovoltaic system

The system incorporates a photovoltaic array delivering 230Wp associated to a buck converter (Fig. 2). The PV output characteristic depends on the temperature (T) and the solar radiation (G) [14]. For these nonlinear PV characteristics, it is necessary to design a Maximum Power Point Tracking (MPPT).

2.1.1. Buck converter sizing

Before integrating MPPT controller, it is essential to properly size the capacitors (C_{pv} , C_{out}) and the inductor (L_{pv}) as shown in Fig. 2 [15].

The converter components sizing (C_{out} , L_{pv}) are based on the following criteria [15]:

- The ripple output current (ΔI_L) must be bigger than 1% of the inductance current (I_L).
- The ripple output voltage (ΔV_{bus}) is required of about 1% of the output voltage (V_{bus}).

Thus L_{pv} and C_{pv} are written as follows:

$$L_{pv} = \frac{D(1-D)V_{pv}}{f\Delta I_L} \tag{1}$$

$$C_{out} = \frac{D(1-D)V_{pv}}{8f^2L_{pv}\Delta V_{bus}} \tag{2}$$

Where f is the pulse width modulation (PWM) frequency equal to 10 kHz, D is the buck converter duty cycle equal to V_{bus}/V_{pv} and V_{pv} is the PV output voltage.

Taking account of the ripple PV output voltage to be less than 2% of its average value, the input capacitor value C_{pv} can be calculated by the following equation [15]:

$$C_{pv} = \frac{D(1-D)I_s}{0.02V_{pv}f} \tag{3}$$

Where I_s is the converter output current.

On the basis of the previous conditions and equations, inductance and capacities values are as follows:

$$L_{pv} = 330\mu\text{H}, C_{pv} = 400\mu\text{F} \text{ and } C_{out} = 50\mu\text{F}.$$

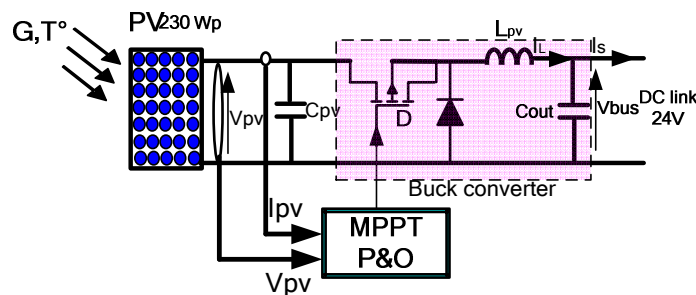


Fig. 2. PVS connected to a dc-dc converter.

2.1.2. MPPT control

The MPPT controller allows the buck converter to track the maximum power as quickly as possible, irrespective of solar radiation.

Several techniques of MPPT have been considered in PV power applications. The Perturbation and Observation (P&O) method is adopted for its simplicity and its fast response time as shown in Fig. 3[11],[14],[15],[16].

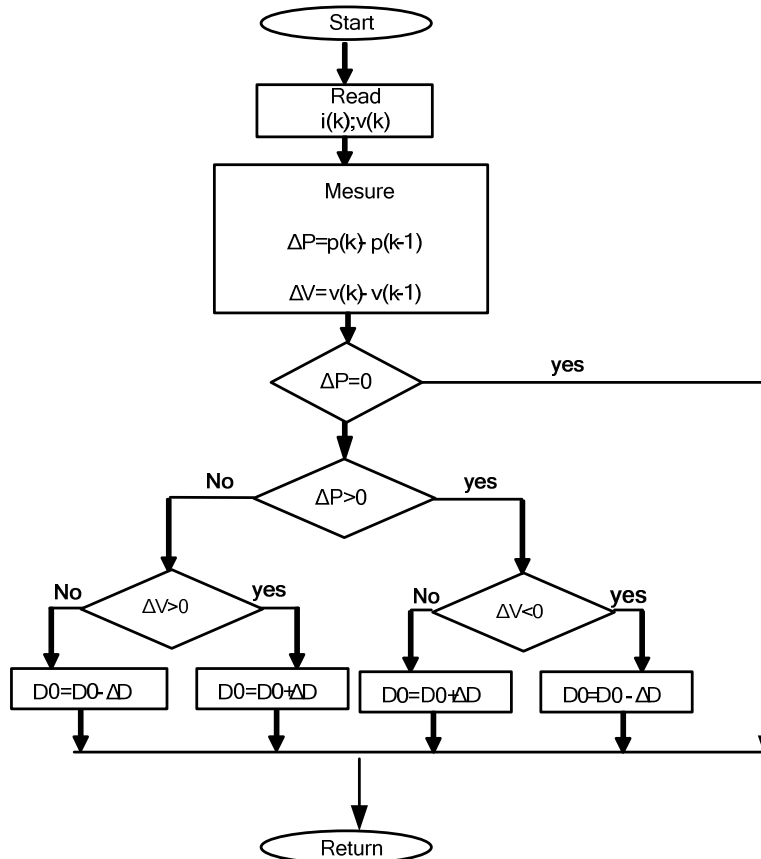


Fig. 3. Perturbation and Observation algorithm flowchart.

2.1.3. Simulation results

The simulation system has been completed for a varying solar radiation from 500 W/m² to 1000 W/m².

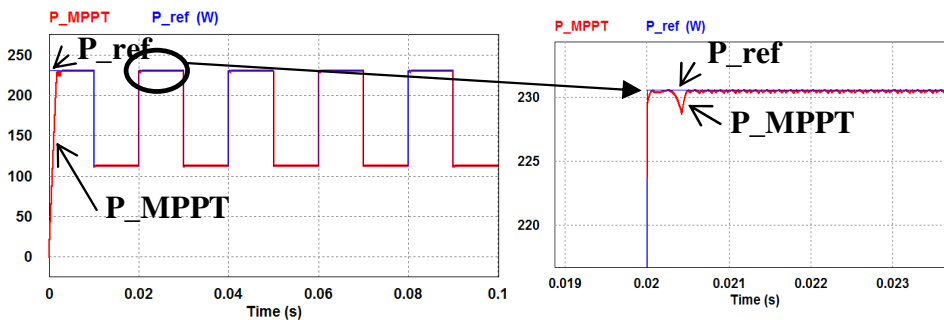


Fig. 4. PVS response for variable radiation.

Erreur ! Source du renvoi introuvable. 4 shows the power output curve of the P&O-MPPT compared to the reference power P_{ref} . These results confirm the performance and the robustness of the P&O algorithm to radiation variations: Power follows the reference value (P_{ref}) with fast response time (0.5ms).

The MPPT design is validate experimentally as shown in Fig. 5.

The experimental test conditions are a variable load and a fixed radiation (337 W/m²).

At the left of the Fig. 5, it's presented the simulation curve. We note that for the given radiation, the PV power should be fixed at 74 Wp. The experimental results are presented at the right. The PV power is effectively equal to 74 Wp (PV curve). The difference between PV and load power is covered with battery curve which presents the battery supply.

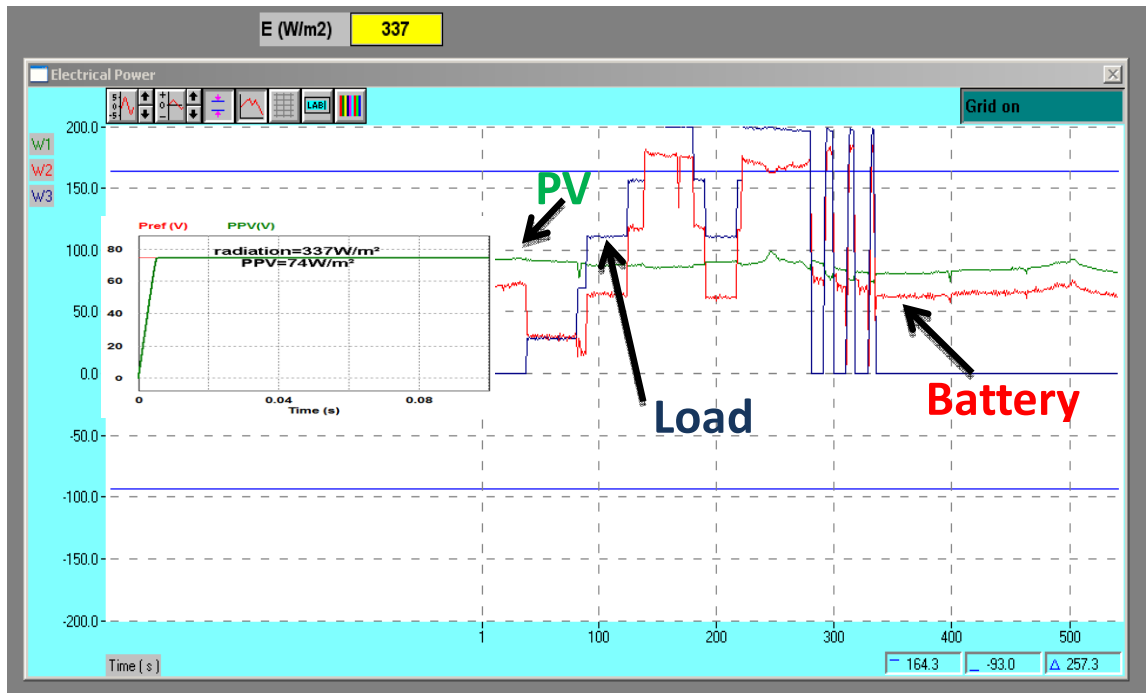


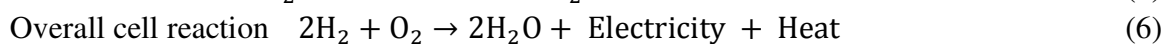
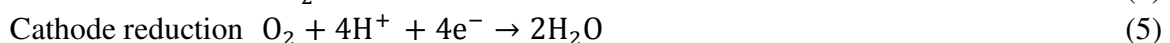
Fig. 5. PVS experimental results.

2.2. Fuel cell system

As mentioned previously, an additional source is required as a supply power during critical conditions (solar radiations are very weak). To accomplish this object, a simple PEMFC model is integrated to design management algorithm for hybrid power system. The proposed simple FC model is detailed in the following.

2.2.1. Fuel cell Model

Fuel cell is an electrochemical device which produces electricity, heat and water from the chemical reactions given by (4), (5) and (6):



The adopted mathematical FCS model is presented in Fig. 6. The model is composed of serial associated continues source E_{th} , ohmic resistance R_{ohm} and two variable voltage sources V_{act} and V_{conc} that are modeling fuel cell losses. V_{cell} is the fuel cell output voltage. The proposed model takes into consideration the operating design parameters and physical material properties.

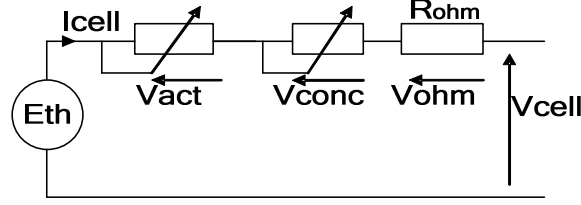


Fig. 6. Proposed electric fuel cell model.

The DC source E_{th} is the theoretical thermodynamic potential incorporating the effect of gas pressures and temperature and it is governed by the Nernst equation (7) and given by [8]-[10].

$$E_{th} = E_0 + \frac{RT}{2F} (\ln(P_{H_2}) + \frac{1}{2} \ln(P_{O_2})) \quad (7)$$

Where E_0 is the fuel cell reversible no loss voltage, R , T and F are respectively the molar gas constant (8,3144 J/mol K), temperature ($^{\circ}$ K) and the faraday's constant (96,485 C/mol). P_{H_2} and P_{O_2} are reactants partial pressures.

The activation losses (V_{act}), the concentration losses (V_{conc}) and the ohmic losses (V_{ohm}) are given by the following equations:

$$V_{act} = \frac{RT}{2\alpha f} \ln\left(\frac{I_{cell}}{I_0}\right) \quad (8)$$

$$V_{conc} = -\frac{RT}{2f} \ln\left(1 - \frac{I_{cell}}{I_{max}}\right) \quad (9)$$

$$V_{ohm} = I_{cell} R_{ohm} \quad (10)$$

Where:

$$R_{ohm} = R_c + R_{memb} \quad (11)$$

And

$$R_{memb} = \frac{l}{\sigma S} \quad (12)$$

Where

$$\sigma = (0.005139\lambda_m - 0.00326)e^{1268(\frac{1}{303} - \frac{1}{T})} \quad (13)$$

where α is the transfer coefficient, I_{cell} the current, I_0 the exchange current, I_{max} the limit current, R_{memb} the resistance of the membrane, R_c the contact resistance, l the membrane thickness and S the fuel cell area.

Also, the Nafion 117 conductivity σ is presented in (13), where λ_m the hydration level considered as constant and the membrane resistance is given by (12).

The different parameters of the proposed model (I_0 , I_{max} , R_c , E_0 , α) are extracted from experimental measurements detailed in 2.2.3.

The cell voltage output (V_{cell}) is presented by:

$$V_{cell} = E_{th} - V_{conc} - V_{act} - V_{ohm} \quad (14)$$

The global FC is composed of N cells, thus V_{fc} is given as follows:

$$V_{fc} = N(E_{th} - V_{conc} - V_{act} - V_{ohm}) \quad (15)$$

Fig. 7 presents the FC voltage and power as a function of the current I_{cell} according to the proposed model presented in Fig. 6.

The obtained curve is composed of three major domains resultant to: the electrochemical activation polarization for low current (domain 1), a linear part where the voltage drop is due to electronic and ionic internal resistances (domain 2) and the last part where the diffusion kinetics of gases through the electrodes in the limiting factor (domain 3). This last zone is characterized by a sharp voltage fall. The power curve presents a maximum point M (3,7A, 100W). This point corresponds to a voltage of 27V.

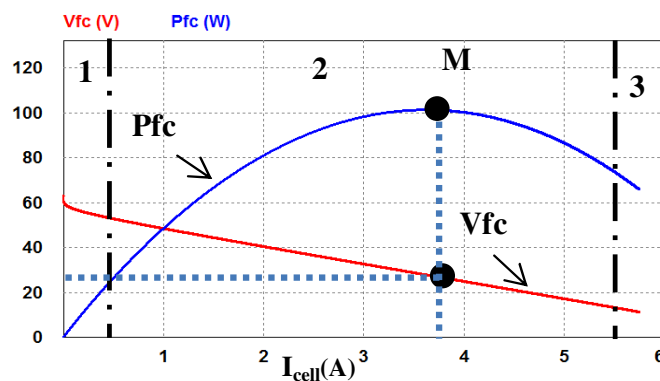


Fig. 7. FC Voltage and power vs. current.

2.2.2. Test bench

The test station presented in Fig. 8 is made in the Photovoltaic laboratory in CRTEn. It allows analyzing and improving the fuel cell performances [17].

For the test bench (Fig. 8), air is supplied from a compressor (b) through a humidification unit (c), and pure hydrogen comes from tanks (a). A cooling system ensures a constant temperature by heating or cooling the water circuit (d). A programmable control item contains all essential control functions, such as measurement conditioning and security shutdown (e).



Fig. 8. FC test bench.

The experimental tests are performed with commercial fuel cell (Fig. 9) provided by [17] and characterized by an active surface of 25 cm². The Nafion membrane thickness is of 178 μm and hydration level λ_m is equal to 14,5.



Fig. 9. Commercial fuel cell.

2.2.3. Fuel cell model identification

The experimental test conditions were carried out under a temperature of 298K, and an operating hydrogen and air pressures equal to 1 bar. The different parameters of the fuel cell are identified from the experimental curve $V_{cell-exp}$ in function of I_{cell} (Fig. 10) and their values are as follows:

$$E_0 = 0,97V ; I_0 = 0,1A ; I_{max} = 7A ; R_c = 0,0003\Omega ; RT / (2\alpha F) = 0,016 .$$

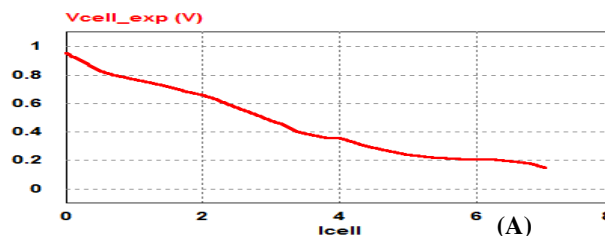


Fig. 10. Experimental FC polarisation curve.

The parameters deduced above are used to plot the theoretical curve V_{cell} in function of I_{cell} using the mathematical model developed in section 2.2.1.

Table 1: FC parameters.

Parameters	Value
E_0	0,97V
I_0	0,1A
I_{max}	7A
R_c	0,0003Ω
$RT/(2\alpha F)$	0,016

The theoretical polarization curve is compared to the experimental one (Fig. 11). The two curves are comparable, which confirm the proposed model validity.

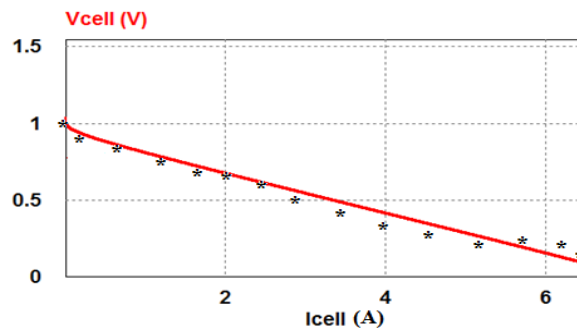


Fig. 11. Experimental (*) and theoretical (-) commercial FC polarization curve.

2.2.4. FC converter control

The aim of the control is to ensure maximum power extracted from the FCS (100W). The FC system is based on a buck converter operating with cascade control loop, as shown in (Fig. 12).

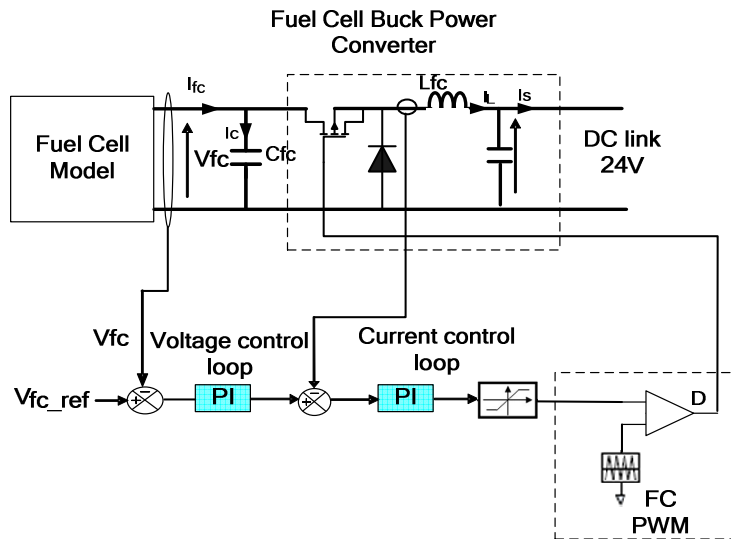


Fig. 12. Fuel cell Control

The cascade control is performed by an external voltage control loop and an internal current control loop, where the PI controller is used.

The simulation results presented in Fig. 13 and Fig. 14 confirm that the proposed controller enables the FCS to supply the maximum power (100W). In fact, when V_{fc} follows its reference value V_{fc_ref} (Fig. 13), the optimal functioning is performed as explained above (Fig. 14).

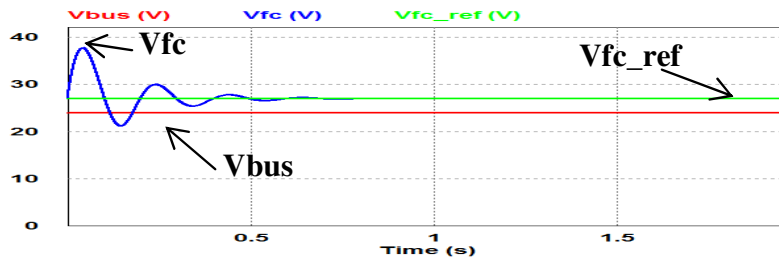


Fig. 13. FCS and DC bus voltages.

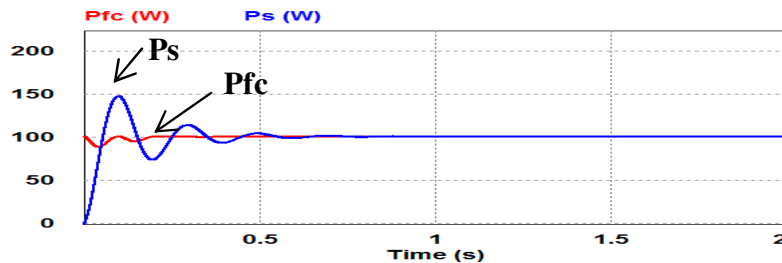


Fig. 14. FC Power supplied.

2.3. BATTERY SYSTEM

The proposed system study the case of residential loads supplied with 24 V. So, the DC link voltage must be maintained at its reference value (24V) which is ensured by the storage system as shown in Fig. 15. The storage system is composed of a battery, connected to the DC bus through a dc-dc bidirectional half bridge converter.

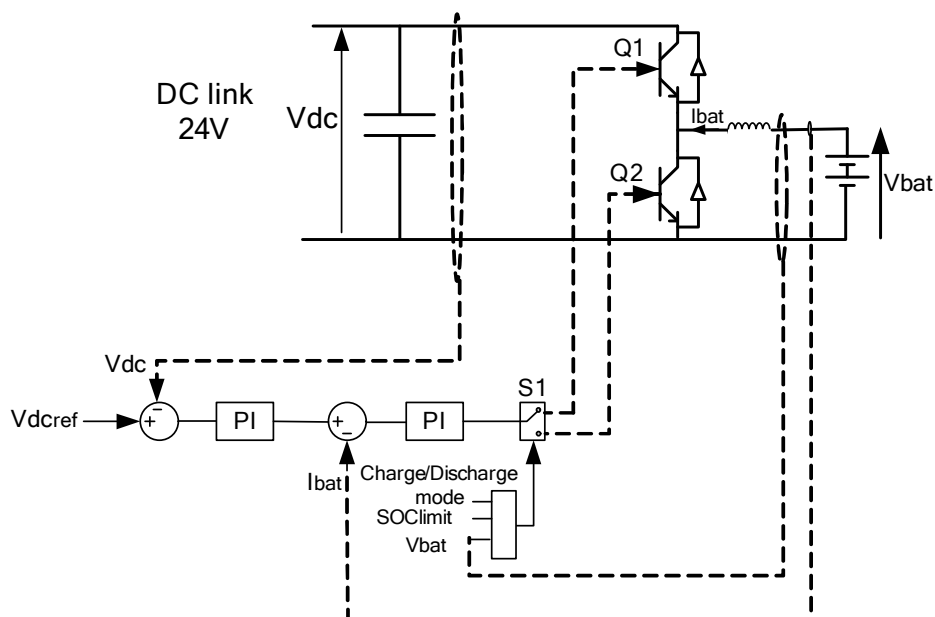


Fig. 15. Battery converter control.

The dc–dc converter operates in boost mode when discharging battery and buck mode when charging it.

The control is achieved by two loops: the external one regulates the DC bus voltage and the internal one regulates the battery current. The control verifies the state of charge (SOC) to avoid damaging the battery.

The used battery is a lead acid whose model is a controlled voltage source in series with an internal resistance expressed as:

$$V_{bat} = E_{bat} - R_i i_{bat} \quad (16)$$

Where V_{bat} (V) is the battery terminal voltage, E_{bat} (V) is the open circuit voltage, R_i (Ω) is the internal resistance (assumed to be constant) and i_{bat} (A) is the battery current. The state of charge (SOC) is calculated as follows:

$$SOC (\%) = 100 \left(1 - \frac{\int i_{bat} dt}{Q} \right) \quad (17)$$

Where Q (Ah) is the maximum battery capacity.

Energy Management of the global system

3.1. MANAGEMENT ALGORITHM

The global system (Fig. 1) includes PVS, FCS and a storage system. The supervision unit has to manage the power to achieve uninterrupted stand-alone operation. It takes into account the various natural conditions, the possibility of non-availability component and the special residential load shape. The flowchart describing the management of the power flow is shown in Fig. 16.

The management unit is based on the principle of introducing the PVS as a primary power system, then the FCS as a secondary system. The battery is considered as a backup power source.

In fact, if the solar radiation level is high enough, the PVS supplies the load as a primary power system and the surplus power is stored in the battery. If the battery maximum state of charge (SOC_{max}) is reached, a dump load is enabled to consume the energy surplus and to maintain the system power balance. Whenever the PV system cannot completely satisfy load demands, the FCS is switched on (Fig. 16)

If the power supplied by the FC-PV combination is lower than the power required by the load, the battery delivers the excess power. In case the battery SOC drops below SOC_{min} , the proposed solution is to shed the secondary loads.

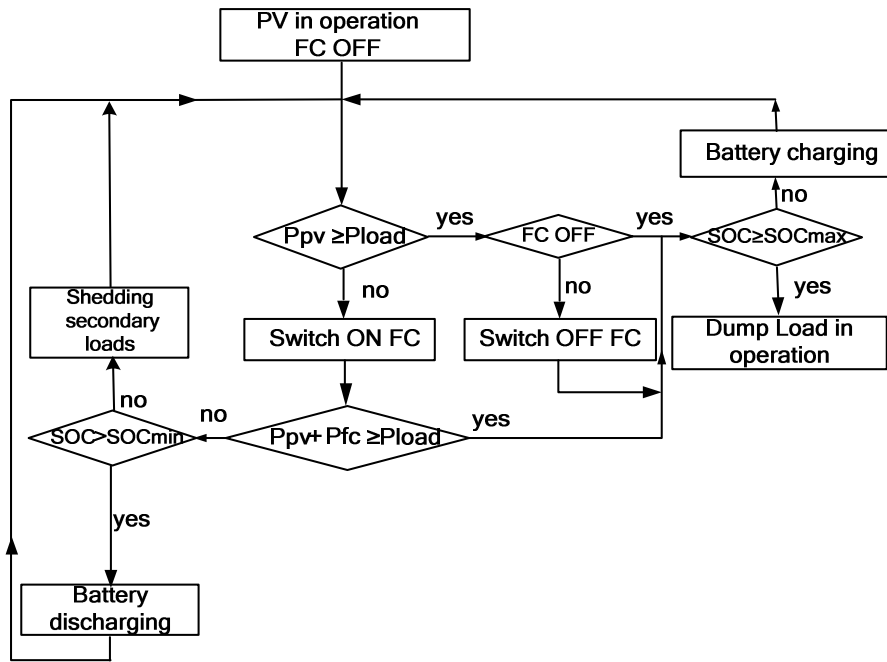


Fig. 16. Energy management flowchart.

3.2. SIMULATION RESULTS

Several scenarios were performed to verify the power management algorithm efficiency. The first test (Fig. 17) concerns the case of fixed radiation and variable load. Between 0 and 0,8 s the PVS power supply satisfies load demand ($P_{pv} > P_{load}$), the energy excess is stored in the battery. From 0,8 s to 1,8s, FCS is switched on to provide energy ($P_{fc} + P_{pv} > P_{load}$), and according to adopted algorithm, the surplus power available from sources is stored in the battery, the battery is in charging mode. From 1,8 s, the power from both sources (PV and FC) becomes insufficient, so the battery is discharging to cover the deficits (discharging mode).

The dc-link voltage presents some fluctuations in each transition step.

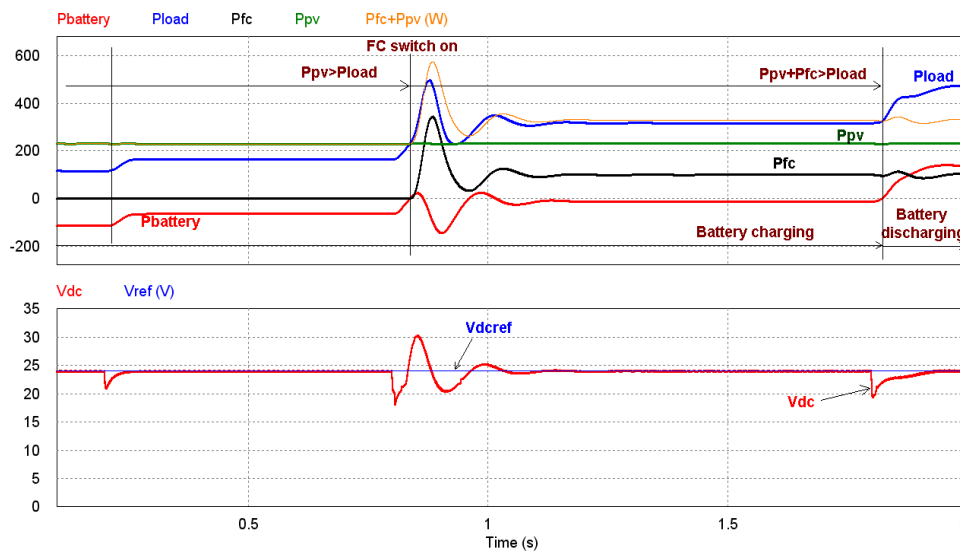


Fig. 17. Power management for fixed radiation and variable load.

Fig. 18 shows the case of variable radiation between 500 W/m^2 and 1000 W/m^2 with fixed load.

During solar radiation variations, it is seen that FC and battery are sustaining the power balance between load demand and PV generation. The DC link voltage is well controlled for intermittent PV power throughout the whole period. It is kept at 24 V.

In each transition, between fluctuation in boost or buck mode, the dc link presents a peak. The positive current indicates the battery discharging mode, that is to say the boost mode of the dc-dc converter. And, the negative current indicates the buck mode of the dc-dc converter.

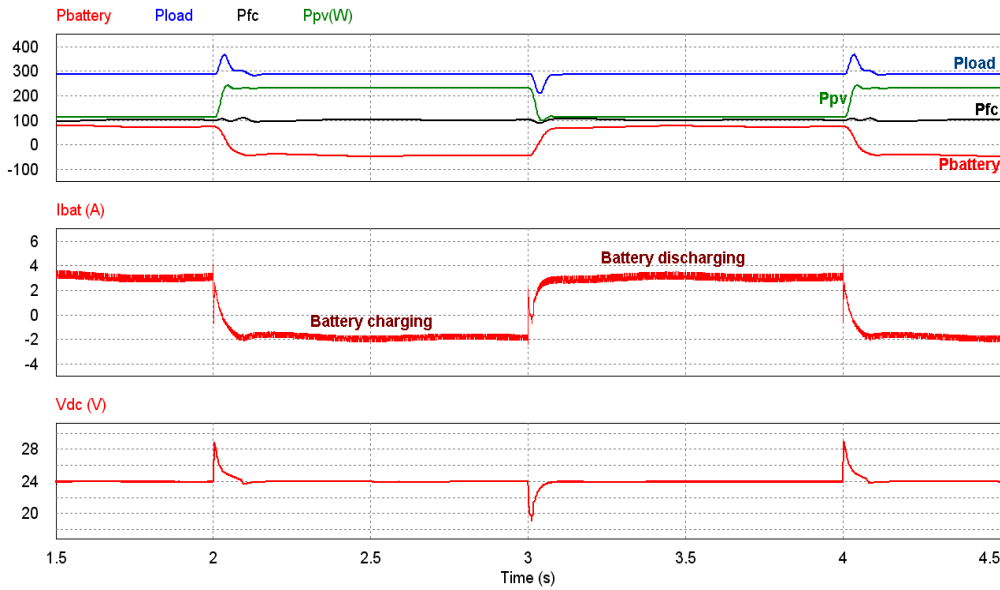


Fig. 18. Case of the variable solar radiation energy for the generation of a fixed charge.

Fig. 19 shows the scenario where the FCS is non-available (failed membrane, empty hydrogen tank). When $P_{pv} < P_{load}$ (from 0,8 s), the battery is switched on to supply load. The corresponding DC-link voltage response is constant.

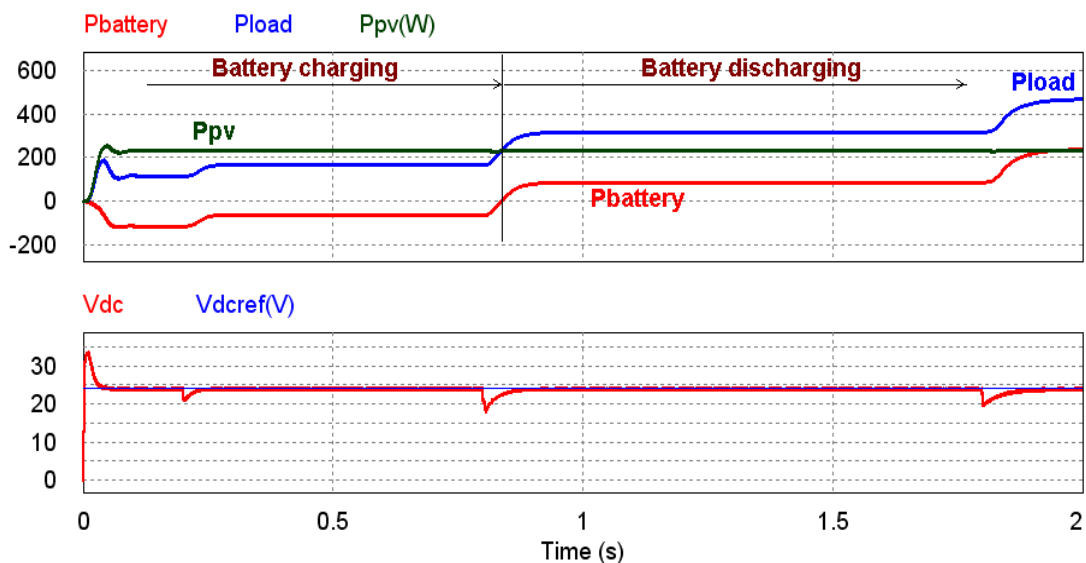


Fig. 19. Energy management in absence of FCS.

Fig. 20 shows the case where the radiation is in its low level or PVS fails, Therefore FCS and battery provide power to the load

Due to its slow dynamics, FC cannot instantaneously meet the rapidly increasing load demand while the battery has a fast response. So for starting the system, the battery intervenes to supply load. When FC starts, the battery power decreases and switch to charging mode.

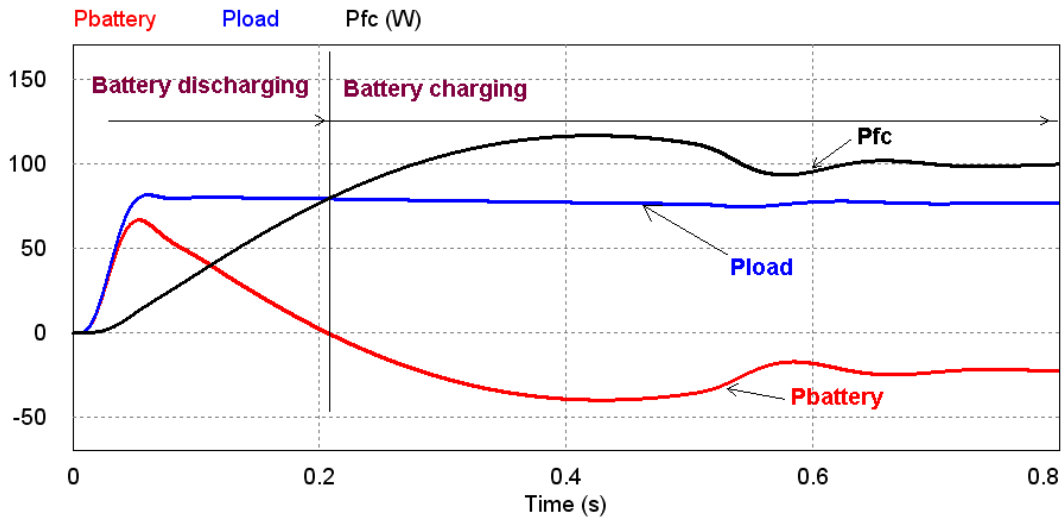


Fig. 20. Energy generation in the absence of PVS.

Fig. 21 shows the case of FC switch OFF. FCS followed by the battery is used to compensate the shortage of the power supplied by the PVS. When the load demand is less than sources power, FCS is deactivated according to the adopted algorithm. Therefore, PVS is sustaining the load demand and the surplus is stored in the battery.

The FC system has slow dynamic when switching OFF at 0,85 s. So, the battery intervenes to improve FC dynamic behaviors.

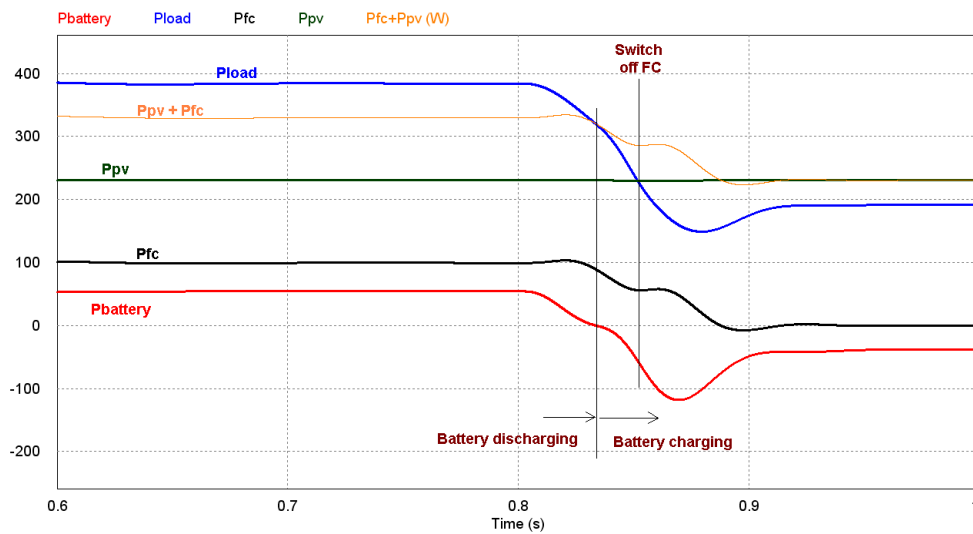


Fig. 21. Case of FC switching OFF

4. Conclusion

This paper presented a simple FC model for the design and control of an hybrid system that guarantees the energy continuity in residential stand-alone mode. The hybrid system includes PV, FC and battery storage device. The proposed FC model is an electrical circuit model whose parameters are experimentally identified. Model validation is performed by comparing simulation results with corresponding experimental polarization curves. Then, a power management algorithm is performed to test the proposed FC model when integrated into the hybrid system. Many scenarios are presented to verify the validity of the power management algorithm, taking into account various meteorological conditions and non-availability PV or FC system.

Acknowledgment

This work was supported by the Tunisian Ministry of High Education and Research under Grant LSE-ENIT-LR11ES15 and CRTEn- LR10CRTEn01 under Europe-Tunisia Cooperation project (ETRERA) and Tunis-Egypt collaboration project 62/4/10.

References

- [1] F. Gao, B. Blunier, M.G. Simoes, A. Miraou, PEM Fuel Cell Stack Modeling for Real-Time Emulation in Hardware-in-the-Loop Applications, *IEEE Transactions on Energy Conversion* 26, 184 – 194, 2011.
- [2] M. Hattia, M. Meharrarb, M. Tioursic, Power management strategy in the alternative energy photovoltaic/PEM Fuel Cell hybrid system, *Renew. Sust. Energ Rev*, 5104– 5110, 2011.
- [3] Wei, Modeling Control and simulation of a PV/FC/UC based hybrid power generation system for stand-alone applications, *IEEE Transactions on Power Electronics* 22, 670-678, 2009.
- [4] E. Mbarek, J. Belhadj, Photovoltaic wind hybrid system integrating a Permanent Exchange Membrane Fuel Cell (PEMFC), *International Conference on Systems, Signals and Devices Tunisia*, pp.1-6, 2009.
- [5] J. Lagorse, D. Paire, A. Miraoui, Hybrid stand-alone power supply using PEMFC, PV and battery - Modeling and optimization, *Conference on Clean Electrical Power*, pp. 135 – 140, 2009.
- [6] X. Li, Design and control of bi-directional DC/DC converter for 30kW Fuel Cell power system, *IEEE 8th International Conference on Power Electronics Asia (ICPE 2011)*, pp. 1024 – 1030, 2011.
- [7] A. Naik, R.Y. Udaykumar, V. Kole, Power management of a hybrid PEMFC-PV and ultracapacitor for stand-alone and grid connected applications, *IEEE International Conference on Power Electronics, Drives and Energy Systems (PEDES 2012)*, pp.1 – 5, 2012.
- [8] G. Fontes, C. Turpin, S. Astier, T.A. Meynard, Interactions Between Fuel Cells and Power Converters: Influence of Current Harmonics on a Fuel Cell Stack, *IEEE Transactions on Power Electronics* 22, 670-678, 2007.
- [9] H.J. Avelar, E.A.A. Coelho, J.R. Camacho, J.B. Vieira Junior, L.C. Freitas, W.U. Marcel, PEM Fuel Cell Dynamic Model for Electronic Circuit Simulator, *IEEE Electrical Power & Energy Conference*, pp.1 – 6, 2009.
- [10] J.S. Kim, G.Y. Choe, B.K. Lee, J.S. Shim, Advanced Interchangeable Dynamic Simulation Model for the Optimal Design of a Fuel Cell Power Conditioning System, *J. Electr. Eng. Technol* 5 (2010) 561–570.
- [11] M. Andujar, F. Segura, M.J. Vasallo, A suitable model plant for control of the set Fuel Cell_DC/DC converter, *Renew. Energy* 33, 813–826, 2008.
- [12] P.N. Papadopoulos, M. Kandyla, P. Kourtza, T.A. Papadopoulos, G.K. Papagiannis, Parametric analysis of the steady state and dynamic performance of proton exchange membrane fuel cell models, *Renew Energy* 71, 23-31, 2014.
- [13] J. Kuo, C. Wang, An integrated simulation model for PEM Fuel Cell power systems with a buck DC-DC converter, *Int. J. Hydrogen Energy*, 11846–11855, 2011.
- [14] M. Sheraz Khalid, M.A. Abido, A novel and accurate photovoltaic simulator based on seven-parameter model, *Elect. Power Syst. Res* 116, 243–251, 2014.
- [15] M. Hatti, Controleur Flou pour la Poursuite du Point de Puissance Maximum d'un Systeme Photovoltaique, *Conference of Young Researchers in Electrical Engineering*, pp.1 – 6, 2008.
- [16] A.R.Saxena, S.M.Gupta, Performance Analysis of P&O and Incremental Conductance MPPT Algorithms Under Rapidly Changing Weather Conditions, *J. Electrical Systems* 10(3), 292-304, 2014.
- [17] M. Barbouche, H. Gobantini, Design and realization of fuel cell test station, *International Renewable Energy Congress Tunisia*, pp.271- 276, 2011.